Monthly Notices
of the
ROYAL ASTRONOMICAL SOCIETY
MNRAS **457,** 3372–3383 (2016) doi:10.1093/mnras/stv3000

Physical parameters and long-term photometric variability of V1481 Ori, an SB2 member of Orion nebula Cluster with an accreting component

S. Messina,[1⋆] P. Parihar,[2⋆] K. Biazzo,[1⋆] A. F. Lanza,[1] E. Distefano,[1] C. H. F. Melo,[3] D. H. Bradstreet[4] and W. Herbst[5]

[1]*INAF – Catania Astrophysical Observatory, via S.Sofia 78, I-95123 Catania, Italy*
[2]*Indian Institute of Astrophysics, Bangalore 560034, India*
[3]*ESO – European Southern Observatory, Alonso de Cordova 3107, Vitacura Casilla 19001, Santiago 19, Chile*
[4]*Eastern University, St Davids, PA 19087, USA*
[5]*Astronomy Department, Wesleyan University, Middletown, CT 06459, USA*

Accepted 2015 December 22. Received 2015 December 18; in original form 2015 October 9

ABSTRACT

We present the results of our analysis on V1481 Ori (JW 239), a young SB2 in the Orion nebula Cluster with a circumbinary disc accreting on the lower mass component. The analysis is based on high-resolution spectroscopic data and high-quality photometric time series about 20-yr long. Thanks to the spectroscopy, we confirm the binary nature of this system consisting of M3 + M4 components and derive the mass ratio $M_B/M_A = 0.54$, a variable luminosity ratio $L_B/L_A = 0.68$–0.94, and an orbital period $P_{orb} = 4.433$ d. The photometric data allowed us to measure the rotation periods of the two components $P_{phot} = 4.4351$ d and they are found to be synchronized with the orbital period. The simultaneous modelling of *V*-, *I*-band, and radial velocity curves in the 2005 season suggests that the variability is dominated by one hotspot on the secondary component covering at least ∼3.5 per cent of the stellar surface and about 420 K hotter than the unperturbed photosphere. Such a spot may originate from the material of the circumbinary disc accreting on to the secondary component. We also detect an apparent 6-yr periodic variation in the position of this hotspot, which is inferred from the phase migration of the light-curve maximum, which we interpret as due to either the presence of surface differential rotation as large as 0.065 per cent, a value compatible with the fully convective components, or to a periodic exchange of angular momentum between the disc and the star, which implies a minimum magnetic field strength of 650 G at the stellar surface.

Key words: binaries: spectroscopic – circumstellar matter – stars: individual: V1481 Ori – stars: late-type – stars: low-mass – stars: pre-main-sequence.

1 INTRODUCTION

Close binary systems with low-mass components in star-forming regions are valuable astrophysical laboratories to address a number of important issues such as accretion, differential rotation, and rotation synchronization. Current models of accretion processes make different predictions (see, e.g. Artymowicz & Lubow 1996; de Val-Borro et al. 2011) about the component(s) on which the accretion takes place, especially in the case the components have different masses. A comparison of model results with real cases is, therefore, highly useful.

Another important issue concerns the presence of differential rotation. The components of the system are fully convective yet, and, on theoretical grounds, the rotation state is expected to be very close to a rigid-body state (see, e.g. Küker & Rüdiger 1997). As a consequence, the stellar magnetic field is likely to be generated by a distributed dynamo like the α^2 dynamo, rather than an $\alpha\Omega$ dynamo. The field geometry is expected to be non-axisymmetric and to show no cyclical behaviour. Moreover, Küker & Stix (2001), modelling the differential rotation of the Sun, derived its Pre-Main-Sequence (PMS) evolution, and found that the total shear $\delta\Omega$ on the Hayashi track is small and it depends on spectral type rather than on rotation rate. The lower the effective temperature the more rigid the rotation (see, e.g. Barnes et al. 2005; Collier Cameron 2007). These expectations are supported by our own analysis as well as by other earlier observational studies (e.g. Johns-Krull 1996; Rice & Strassmeier 1996) that did not detect any significant evidence for surface differential rotation (SDR) in classical T Tauri (CTTS) stars. For example, Cohen, Herbst & Williams (2004), basing their analysis on an approximately 4 yr long time series data of a sample of IC

⋆ E-mail: sme@oact.inaf.it (SM); psp@iiap.res.in (PP); kba@oact.inaf.it (KB)

348 members (∼2–3 Myr), neither detect clear evidence of activity cycles nor of photometric rotation period variations attributed to differential rotation. However, persistent spots that do not migrate may be responsible for the SDR non-detection.

Another interesting issue concerns the time-scale for the synchronization of the rotation of the system's components with the orbital period. To address this, we require measurements of photometric rotation periods of both components and of the orbital period.

A few such interesting close binary systems have been monitored spectroscopically and photometrically over a long time base as a part of a programme focused on young stellar objects in the Orion nebula Cluster (ONC) begun by Parihar and collaborators in 2004 (Parihar et al. 2009), using the facilities available at the Indian Astronomical Observatory (IAO). A number of the ONC members monitored at IAO have been also photometrically monitored at the Van Vleck Observatory (VVO) on the campus of Wesleyan University since 1991 by Herbst and collaborators (see, e.g. Herbst et al. 2000). These two monitoring programs have provided us with a photometric data time series almost 20 yr long for about 100 ONC members. The data collected over such a long time span, together with spectroscopic data, allow us to explore the accretion processes, presence of SDR, and rotation/orbital period synchronization.

In this paper, we report the results obtained for one interesting ONC cluster member – the spectroscopic binary V1481 Ori. We find that this system exhibits periodic photometric variations that may originate from the presence of an accretion hotspot on the photosphere of the secondary component. The hotspot is carried in and out of view by the stellar rotation and produces periodic flux enhancements. Although the system does not exhibit any evidence of photometric rotation period variation, unexpectedly, it shows a periodic variation of the phase of the light-curve maximum. This oscillation of the phase of maximum may arise from a variation of the angular velocity due to a periodic latitude migration of the hotspot on a differentially rotating star. An alternative explanation is that the disc and the star exchange angular momentum back and forth in a cyclic fashion.

The literature on V1481 Ori is reviewed in Section 2, the spectroscopic and photometric observations are presented in Section 3, the photometric analysis is in Section 4, and the derived orbital and physical parameters are given in Section 5. Discussion and conclusions are presented in Sections 6 and 7.

2 V1481 ORI

V1481 Ori (α = 05:35:03.92, δ = −05:29:03.35, J2000.0; V = 15.45 mag, $V-I$ = 2.40 mag) is a low-mass member of the ONC. First catalogued with sequential number 1725 by Parenago (1954) in his survey of stars in the Orion nebula area, it was subsequently discovered to be variable by Rosino (1956) from analysis of photographic plates. Jones & Walker (1988), who assigned the number JW 239, also found evidence of variability. The rotation period P = 4.46 d was first measured by Edwards et al. (1993), after this star was included in the photometric monitoring program at VVO in 1991 (Attridge & Herbst 1992). It is designated as V1481 Ori in the 76th Name-List of Variable Stars (Kazarovets, Samus & Durlevich 2001).

Basic stellar parameters were first determined by Hillenbrand (1997) who estimated a probability of membership to ONC of 99 per cent, mass $M = 0.24$ M$_\odot$, radius $R = 2.73$ R$_\odot$, effective temperature $T_{\rm eff} = 3590$ K, interstellar absorption $A_{\rm V} = 0.47$ mag, and spectral type M1.5, whereas Edwards et al. (1993) assigned a later ∼M4 spectral type. Da Rio et al. (2010) have estimated a smaller reddening $A_{\rm V} = 0.33$ mag and a larger mass $M \simeq 0.41$ M$_\odot$. However, all these measurements referred to the unresolved system. Recently, V1481 Ori was discovered to be an SB2 system by Tobin et al. (2009). Biazzo et al. (2009) found additional evidence of its binary nature from a cross-correlation function analysis, and derived the following values for the projected rotational velocities of the two components: $v \sin i_{\rm A} = 19.2 \pm 1.1$ km s^{-1} and $v \sin i_{\rm B} = 16.1 \pm 0.9$ km s^{-1}. V1481 Ori exhibits variable Hα line emission: Equivalent Width (EW) = −13.0 Å (in 2004 March; Sicilia-Aguilar et al. 2005), +0.44 Å (in 2005 January; Da Rio et al. 2009), −12.75 Å (in 2007 February; Parihar et al. 2009), and −17.7 Å (Furesz et al. 2008).

The possible presence of a disc is indicated by near-infrared excess in both Two Micron All-Sky Survey (2MASS) and Infrared Array Camera (IRAC)/*Spitzer* photometry (Werner et al. 2004). Rebull et al. (2006) measure a value of [3.6] − [8] = 1.3 mag, indicative of an active accretion disc, and found hint that the accretion was variable. Based on these results, they classified it as CTTS. On the other hand, other measurements do not show any excess, like the values of $\Delta[I-K] = -0.03$ mag measured by Rodriguez-Ledesma, Mundt & Eisloeffel (2010), or $\Delta[I-K] = 0.38$ mag by Hillenbrand et al. (1998), which is a value very close to the boundary adopted to distinguish disc from disc-less stars. The more recent *Wide-field Infrared Survey Explorer* observations (Cutri et al. 2013) demonstrate a prominent IR excess, leaving no doubt about the presence of an accretion disc.

V1481 Ori is also an X-ray source, first detected by the *ROSAT* satellite as part of surveys of ONC (Gagne, Caillault & Stauffer 1995; Geier, Wendker & Wisotzki 1995), and subsequently by the *Chandra* satellite (Feigelson et al. 2002; Getman et al. 2005).

3 OBSERVATIONS

3.1 Spectroscopy

The spectroscopic observations of V1481 Ori were obtained in Period 76A at the European Southern Observatory (ESO)/Very Large Telescope (VLT) (Chile). Spectra were collected within the FLAMES (Fibre Large Array Multi-Element Spectrograph) Guaranteed Time Observers with the multi-object GIRAFFE spectrograph in MEDUSA mode.[1] One of these spectra was analysed by Biazzo et al. (2009) with the aim to study the disc-locking scenario for low-mass stars in the ONC. Observations were carried out in 2005–2006 from October 15th to January 20th (∼8.4 h on 11 nights). The HR15 GIRAFFE setup ($R \sim 19\,300$, λ = 659.9–695.5 nm) was chosen. The log of spectroscopic observations is given in Table 1. A total of 11 spectra of V1481 Ori were obtained and reduced using the GIRAFFE Base-Line Data Reduction Software (GIRBLDRS; Blecha et al. 2000). Sky subtraction was applied following the prescriptions reported in Biazzo et al. (2009).

3.2 Photometry

The photometric analysis is based on observations collected during two in-progress monitoring programs of ONC members. The first and longest one is the program carried out by Herbst and collaborators at the VVO since 1991 (see, e.g. Herbst et al. 2000). The

[1] This is the observing mode in FLAMES in which 132 fibres with a projected diameter on the sky of 1.2 arcsec feed the GIRAFFE spectrograph. Some fibres are set on the target stars and others on the sky background.

Table 1. Log of spectroscopic observations.

Date (d/m/y)	UT (h:m:s)	t_{exp} (s)
15/10/2005	07:34:35.6	2820
16/10/2005	07:21:02.3	2820
17/10/2005	07:23:30.4	2820
18/10/2005	06:48:58.4	2054
19/10/2005	07:23:01.9	2820
20/10/2005	07:17:21.2	2820
21/10/2005	06:43:17.8	2820
04/11/2005	06:25:09.4	2820
05/11/2005	05:05:07.5	2820
18/01/2006	03:28:52.9	2820
20/01/2006	04:05:21.6	2820

second and more recent one is the observing program carried out by Parihar and collaborators at the IAO since 2003 (see Parihar et al. 2009).

In order to get a homogeneous time series of *I*-band magnitudes, we proceeded as follows. We selected first the time intervals during which both IAO and VVO photometry were almost contemporary (in the years 2004 and 2005). Then, we folded the light curves with the already-known rotation period (from Herbst et al. 2000) and, finally, added a magnitude offset to the VVO data to match with the IAO light curves with the aim to minimize the magnitude dispersion versus rotation phase. This offset $\Delta I = 0.04$ mag arises from either difference between the Johnson–Cousin filter at VVO and Bessel filter at IAO and the uncertainty on the magnitude standardization. The same magnitude offset was applied to all VVO data.

In 1994 December, V1481 Ori was simultaneously observed at VVO and by Stassun et al. (1999) with the 1-m telescope at the Wise Observatory, as part of an independent program. As previously done, we added an offset to the differential magnitudes by Stassun et al. (1999) in order to minimize the magnitude dispersion versus rotation phase with respect to the VVO data. In the end, the precision with which photometric sets coming from different telescopes were combined together was comparable to the average photometric precision of each independent data set.

We applied a 3σ clipping filter to remove outliers on each seasonal time series, where σ is the standard deviation of the seasonal magnitude time series. In principle, some outlier may represent a flare event. However, for the purposes of the present study we focused on only variability arising from the rotational modulation. Then, we averaged observations collected within a time interval of 1 h. More details on the data reduction are given in Parihar et al. (2009) and Herbst et al. (2000).

Our final data set consists of 1552 measurements spanning a time interval of about 20 yr from 1991 October to 2011 March. A summary of the observations is given in Table 2. The complete photometric time series (Heliocentric Julian Day (HJD) versus *I* magnitude) is made available as online Table. In the years from 2004 to 2011, we obtained contemporary *V*- and *I*-magnitude time series at IAO, and also *R* magnitudes during the 2008 season.

4 PHOTOMETRIC ANALYSIS

4.1 Correlation analysis

The multiband observations collected between 2004 and 2008 allow us to infer some additional information on the nature of the observed variability. For each seasonal light curve, we have carried out correlation and linear regression analyses between colours and magnitude variations, which we measured in our light and colour curves, by computing correlation coefficients (r), their significance level (α), and slopes of linear fits (Fig. 1). The significance level α represents the probability of observing a value of the correlation coefficient larger than r for a random sample having the same number of observations and degrees of freedom (Bevington 1969).

We find that the Pearson linear correlation coefficients (r) are larger than 0.90 in every season and their significance levels, α, are larger than 99 per cent. The slopes of the *V* versus *I* variations, derived from linear regression analysis, vary from season to season in the range $dV/dI = 1.24$–1.86 ($dR/dI = 1.40$, $dV/dR = 1.07$ in 2008). Similarly, we computed the slopes of the *V* versus $V-I$ variations and found it to vary in the range $dV/d(V-I) = 1.84$–2.04, with a mean value of 1.89.

Correlation analysis allows us to investigate the origin of magnitude and colour variations. For example, if these variations originate from a single spot or group of small spots, as well as if they originate from two different, but spatially and temporally correlated types of inhomogeneities, e.g. cool spots and hot faculae, we expect these quantities to be correlated. On the contrary, a poor correlation or its absence will tell us that magnitude and colours are affected by at least two mechanisms, which are operating independently from each other, either spatially or temporally. The regression analysis is also important to infer information on the properties of photospheric inhomogeneities, since their averaged temperature mostly determines the slope of the trends. Indeed, surface inhomogeneities with different areas but constant temperature will determine magnitude and colour variation of different amplitude but with a rather constant ratio.

Assuming that magnetic activity is present in both components of V1149 Ori, this circumstance may also play a role in decreasing the expected correlation, since the variabilities arising from the two components are not necessarily correlated. However, we find

Table 2. Summary of *I*-band observations: mean epoch of each light curve, number of measurements, brightest *I* magnitude, light-curve amplitude, and phase of light-curve maximum.

Mean epoch (HJD)	N_m	I_{min} (mag)	ΔI (mag)	Phase of maximum
Complete series				
2452095.979	1522	12.725	0.148	–
2448628.717	22	12.831	0.082	0.822
2449001.119	25	12.786	0.095	0.723
2449359.189	58	12.788	0.104	0.752
2449738.152	183	12.774	0.220	0.816
2450100.182	23	12.784	0.167	0.854
2450448.711	53	12.85	0.095	0.905
2451204.652	13	12.731	0.063	0.659
2451571.158	30	12.717	0.088	0.776
2451882.279	17	12.677	0.147	0.763
2452278.176	24	12.694	0.146	0.833
2452634.223	26	12.72	0.124	0.875
2453022.645	97	12.712	0.074	0.844
2453363.492	77	12.759	0.038	0.704
2453668.802	33	12.734	0.079	0.719
2454132.187	210	12.73	0.144	0.847
2454443.770	404	12.718	0.152	0.880
2454807.325	65	12.63	0.147	0.892
2455170.771	46	12.613	0.169	0.838
2455544.276	69	12.613	0.189	0.783

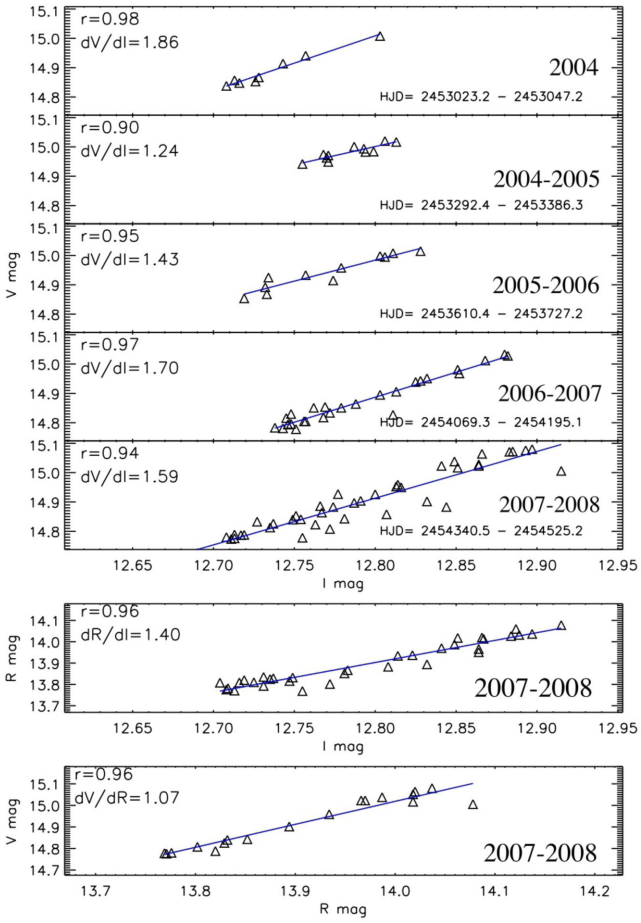

Figure 1. Correlation analysis of *V* versus *I* magnitudes for the observation seasons from 2004 to 2008, and among *I*, *R*, and *V* magnitude for the 2008 season. The correlation coefficients, the slopes of the linear fits, and the date range are plotted as labels.

that the light variations in all bands are strongly correlated, which indicates that either the photometric variability of one component likely dominates over the variability from the other component or they have same periodicities. The spectroscopic analysis in Section 5 will show that the secondary component dominates the observed variability, which arises from a hotspot produced by the infalling gas from the accreting disc. Therefore, in the subsequent analysis we will neglect the contribution to variability by the primary component that will be assumed to be negligible.

The brightest magnitudes and bluest colours of V1481 Ori were observed in the 2010/2011 season and they are $V = 14.62 \pm 0.01$ mag, $I = 12.61 \pm 0.01$ mag, and $V{-}I = 2.01 \pm 0.02$ mag, whereas the faintest and reddest were observed in 1994/1995 and they are $V = 15.45 \pm 0.01$ mag, $I = 13.05 \pm 0.01$ mag, and $V{-}I = 2.40 \pm 0.02$ mag. Therefore, the stars exhibit a variability amplitude of $\Delta V = 0.83 \pm 0.015$ mag, $\Delta I = 0.44 \pm 0.015$ mag, and $\Delta(V{-}I) = 0.39 \pm 0.03$ mag. When modelling the observed magnitude variations, we must keep in mind that they refer to the unresolved system. Therefore, owing to a dilution effect due to the presence of the primary component, which in the present case is a factor 2.18 derived from the magnitude difference between the two components in the *I* band, the total magnitude variations of the secondary component are larger by about the same factor than those observed.

Table 3. Rotation periods derived from periodogram analysis of the *I*-band time series segments.

$HJD_{initial}$	HJD_{final}	P(d)	ΔP	Power	Power @1 per cent FAP
2448539.858	2455267.122	4.43	0.05	164.85	8.23
2448559.812	2448697.569	4.45	0.05	6.85	4.89
2448925.745	2449072.542	4.46	0.07	5.16	4.58
2449280.862	2449434.559	4.44	0.07	22.89	6.21
2449688.734	2449789.552	4.43	0.30	72.53	6.47
2450018.763	2450166.545	4.43	0.07	7.51	6.5
2450369.842	2450523.580	4.43	0.05	11.96	5.22
2451162.753	2451246.552	4.44	0.02	10.91	6.55
2451514.687	2451629.562	4.44	0.07	12.06	5.69
2451838.796	2451931.715	4.44	0.05	6.64	4.89
2452221.728	2452338.596	4.42	0.15	9.67	6.71
2452550.845	2452721.546	4.46	0.16	6.55	5.19
2452960.757	2453079.620	4.43	0.07	15.47	8.08
2453610.425	2453727.179	4.44	0.02	10.91	6.55
2454069.261	2454197.081	4.44	0.07	25.03	6.32
2454339.458	2454548.144	4.43	0.05	42.64	6.73
2454751.446	2454863.204	4.44	0.03	29.88	7.91
2455053.466	2455288.077	4.44	0.02	21.2	5.77
2455436.451	2455652.100	4.44	0.02	30.91	6.55

4.2 Search for rotation period

The light curves of low-mass active stars are known to be characterized by changes of amplitude and shape over different time-scales. During the PMS evolution, Weak-line T Tauri Stars (WTTS) have generally quite stable light curves that maintain similar amplitude and shape for several rotation cycles. On the contrary, CTTS can exhibit significant variations during the same season or from one observation season to the subsequent one, owing to variable accretion phenomena (see, e.g. Grankin et al. 2007, 2008). To search for such variations, we decided to divide the whole time series into a number of segments, corresponding to single observation seasons. Therefore, our analysis was carried out on 19 different light-curve segments as well as on the complete time series (see Table 2).

The period search was carried out using the Lomb–Scargle periodogram (Scargle 1982). The false alarm probability (FAP), that is the probability that a periodicity is not true but simply arises from noise associated to the data, was computed using the bootstrap approach proposed by Herbst et al. (2000), i.e. by generating 1000 artificial light curves obtained from the real one, keeping the date but scrambling the magnitude values. We performed the periodogram analysis on each fake randomized data set and determined the power level corresponding to an FAP = 0.01. We decide to consider only periodicity with FAP < 0.01, that is with confidence level larger than 99 per cent.

In Table 3, we summarize the results of our period search. The same periodicity, which we attribute to the rotation period, was detected with high confidence level in 18 of 19 light curves, as well as in the complete time series. The uncertainty on the period determination was computed following Lamm et al. (2004). In Fig. 2, we display the seasonal time series versus HJD (left column); the periodogram with overplotted (horizontal dashed line) and the power level corresponding to FAP = 0.01 (middle column); the *I*-band light curves phased with the ephemeris HJD = 2453658.8320 + 4.4351 × E (right column). We note that in only one season the period is not detected with FAP < 0.01. None the less, the phased light curve is very smooth and it allows us to accurately determine the phase of maximum. The average rotation period is

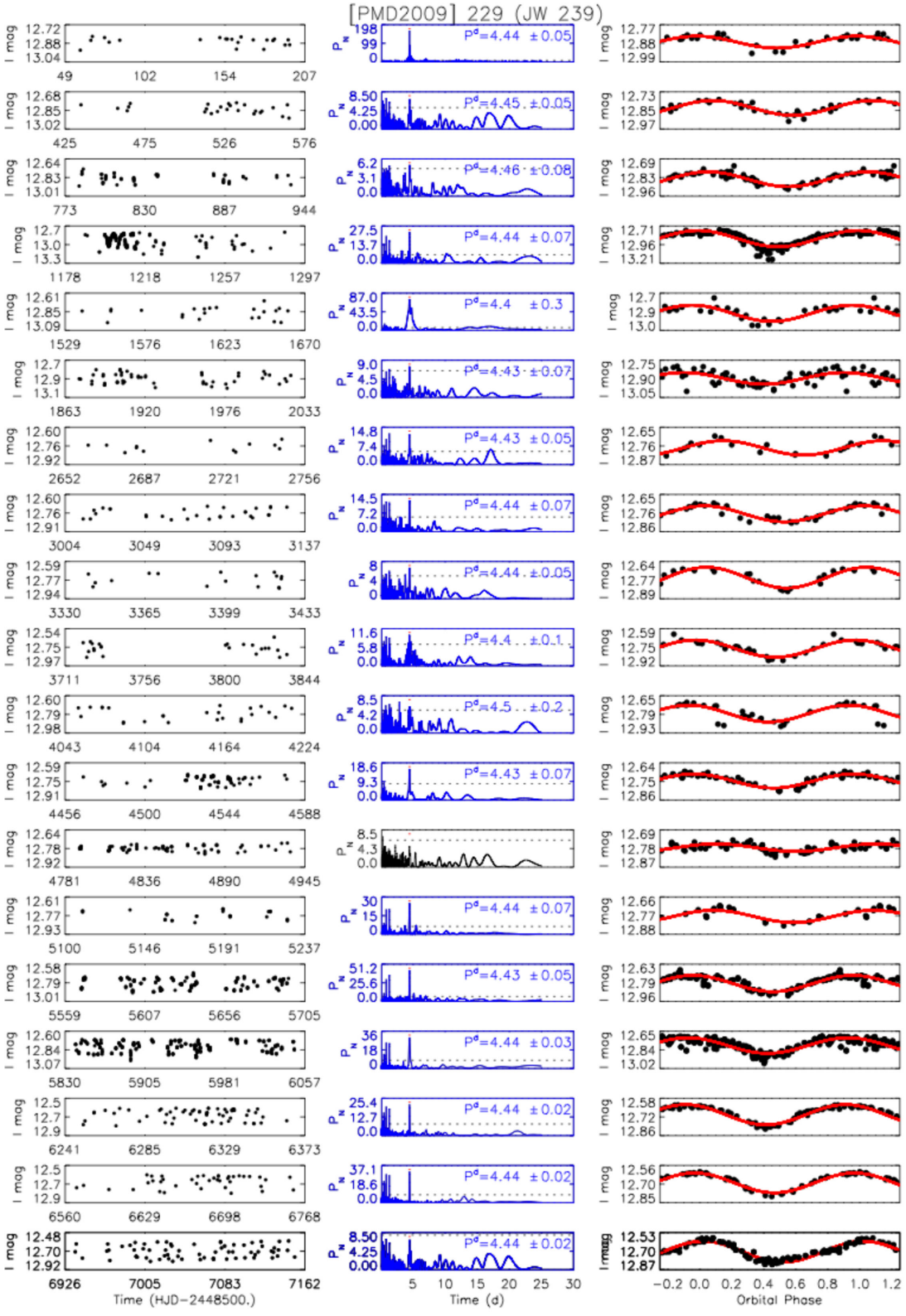

Figure 2. *I*-magnitude time series of V1481 Ori. Left column displays the time segments of magnitudes versus HJD. Middle column displays the Lomb–Scargle periodograms with the 99 per cent confidence level indicated by the horizontal dashed line (black panel indicates no period detection above the 99 per cent confidence level). Right column displays the light curves phased with the ephemeris HJD = 2453658.8320 + 4.4351 × E. Solid lines represent the sinusoidal fit with the rotation period.

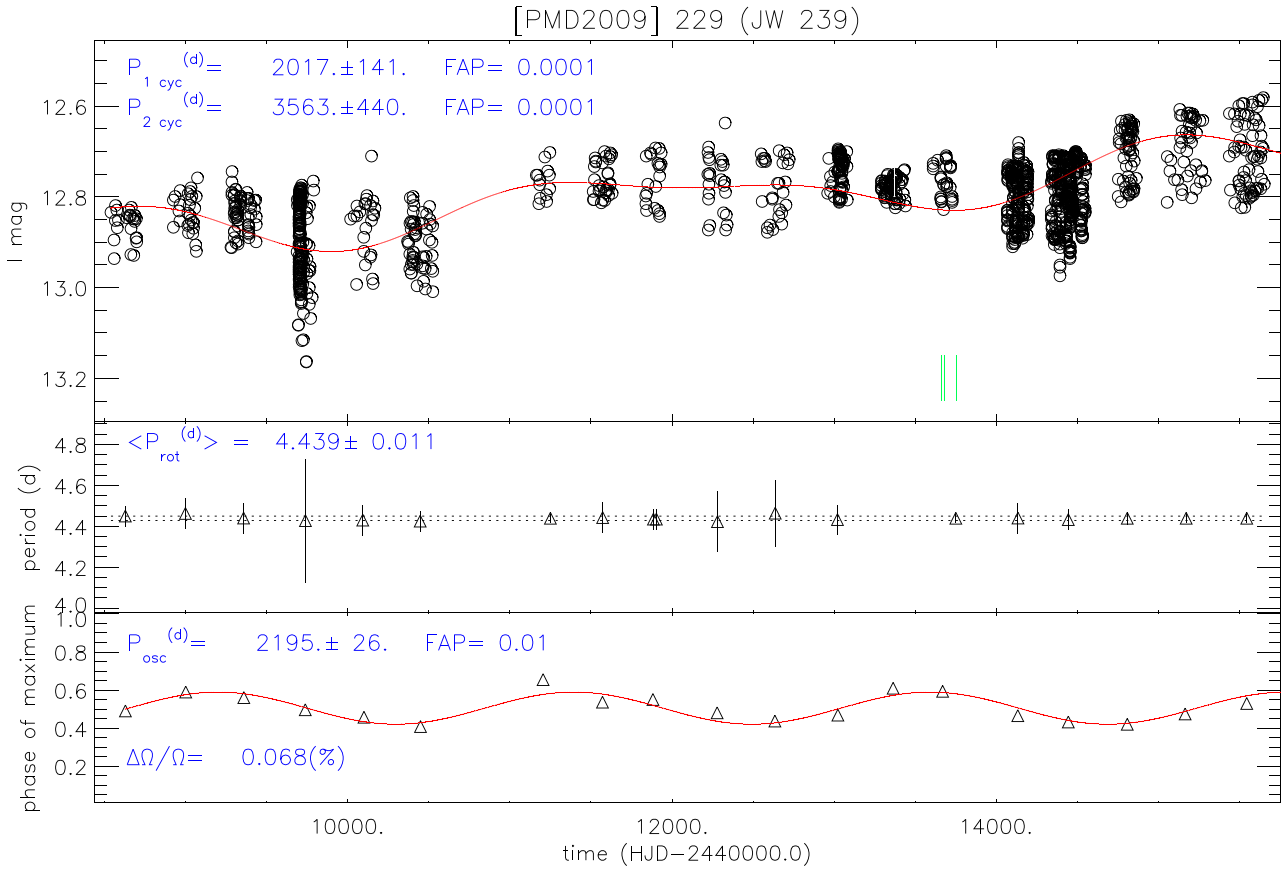

Figure 3. Top panel: *I*-magnitude time series of V 1149 Ori versus time. The solid line represents the sinusoidal fit with the cycle periods of $P_1 = 2046$ d and $P_2 = 3470$ d. Dotted green vertical bars indicate the epochs of spectroscopic observations. Middle panel: time sequence of the seasonal rotation periods listed in Table 3. Dotted lines indicate the 1σ uncertainty on the average period. Bottom panel: phase of the light curve maximum versus time. Solid line represent the sinusoidal fit with the oscillation period $P_{\rm osc} = 2195$ d.

$P = 4.439 \pm 0.011$ d. The largest period variation in the series listed in Table 3 is 0.04 d, which is smaller than the average uncertainty on the period determination (0.05 d). Considering the average period and its uncertainty, all seasonal period determinations differ from the average by less than 2σ. Therefore, we infer that our star does not show any rotation period variation larger than 0.7 per cent, which is the minimum variation at 3σ level detectable by our analysis.

When we plotted the series of 19 light curves using the average rotation period to compute the rotation phases, we noted a linear migration of the phases of light-curve maximum (owing to the presence of hotspots, we consider the light maximum). We made use of the O−C diagram to find the value for which the series of maxima did not exhibit any linear trend (see bottom panel of Fig. 3), and found the following rotation period $P = 4.4351$ d. In the right column of Fig. 2, light curves are phased with the ephemeris HJD = 2453658.8320 + 4.4351 × E. This is the rotation period of the component hosting the hotspot. As we will see from the light-curve modelling and the spectroscopic analysis, the hotspot is hosted by the secondary component. Since the primary component is brighter than the secondary component, its photometric variability is expected to be significant even if the system is not resolved. Now, if the primary component would rotate with a period different that the rotation period of the secondary component, we would expect to find its modulation in the photometric time series. However, we note that neither in the periodogram of the complete photometric series nor in the seasonal periodograms we found evidence for a significant secondary period. Therefore, we can consider that both components have the same rotation that is synchronized with the orbital period. This is particularly interesting because it proves that the components of a close binary can be synchronized during the PMS stage of their evolution. However, we cannot completely rule out the possibility that the primary has a different rotation period, but being quite inactive, although this circumstance is quite unlikely, we do not detect it neither in the light curves nor in the periodograms.

4.3 Pooled variance analysis

We applied also the pooled variance analysis as proposed by Dobson et al. (1990), Donahue & Baliunas (1992), and Donahue, Dobson & Baliunas (1997) to our data time series. The pooled variance is the average variance of the data subsets of length τ. The variance profile plotted in Fig. 4 allows us to identify three characteristic time intervals. The rotational modulation of the flux arising from the presence of active regions produces the first rise of the variance, up to a time-scale about 5 d. The pooled variance stays more or less constant for a time interval from about 5 d up to about 1000 d, that should correspond to the lifetime of the largest surface brightness inhomogeneities. Our photometric times series is not long enough to infer additional information for time-scales longer than 1000 d. Therefore, we confirm that the bright region responsible for the observed variability (which we will show to be the hotspot on the

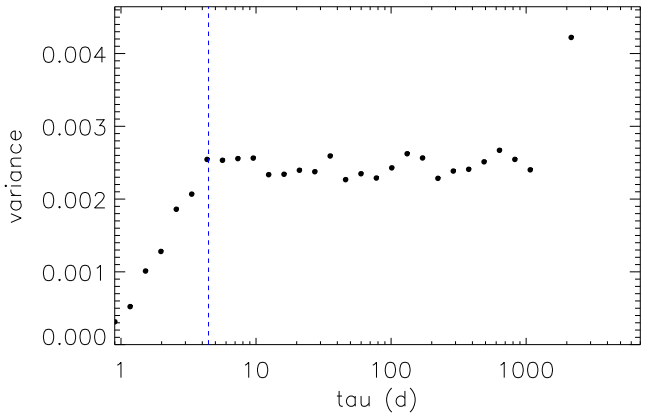

Figure 4. Pooled variance profile of V1481 Ori. The vertical dashed line marks the rotation period.

Table 4. Summary of search for long-term periodic variations: activity indicator, primary/secondary cycle, length of cycle (d), power of the highest periodogram peak, power corresponding to a 99 per cent significance level.

Activity indicator	Cycle	$P \pm \Delta P$ (d)	P_N	$P_{N99\,per\,cent}$
I_{mag}	P_1	2017 ± 141	99	7
	P_2	3563 ± 440	97	7
I_{min}	P_1	3763 ± 76	2.68	1.43
I_{ampl}	P_1	2413 ± 31	6.27	4.50
Phase of maximum	P_1	2195 ± 26	6.5	3.16

accreting secondary component) is quite stable for about 3 yr, which makes the season-to-season variation of the light curve very smooth.

4.4 Search for long-term cycles

The Lomb–Scargle periodogram was also used to investigate the presence of significant long-term periodicities. We computed the periodograms of four different variability indicators: *I*-band magnitudes, brightest and faintest light-curve magnitudes for each light-curve segment, light-curve amplitudes, and phases of light-curve maximum.

We find that our *I*-band magnitude time series displays a long-term increasing linear trend indicating that the system is getting brighter with time. Such a trend may be a segment of a very long activity cycle. Two significant (FAP < 0.01 per cent) periodicities $P_1 = 2017$ d (5.5 yr) and $P_2 = 3563$ d (9.8 yr) are found superimposed to this linear trend. Similar analysis was performed on the series of light curve brightest magnitudes, from which we derived a cycle $P_1 = 3763$ d (10.3 yr), and on the light-curve amplitude, from which we derived a cycle $P_1 = 2413$ d (6.6 yr). The periodogram analysis of the light curve faintest magnitudes did not reveal any significant periodicity. Finally, we made the periodogram of the light-curve phase of maxima and found an oscillation with period $P_{osc} = 2195$ d (6 yr). All these periods have an FAP < 1 per cent. The results are summarized in Table 4. In Fig. 3, we plot the complete time series of *I*-band magnitudes (top panel) overplotted with the linear and sinusoidal fits with the two periods (5.5 and 9.7 yr). In the bottom panel, we plot the phases of maximum overplotted with the sinusoidal fit with the period of 6 yr. We note that our measurements allow us to sample three complete cycles of the phase variation which makes us rather confident that this periodicity may be real. However, a much longer time series is needed to address this issue of possible long-term cycles.

Table 5. RVs of the binary system V1481 Ori (A: primary component; B: secondary component).

JD	V_{rad}^{A} (km s^{-1})	V_{rad}^{B} (km s^{-1})
2453658.8320[a]	24.36 ± 1.25	
2453659.8226	−17.04 ± 1.04	96.34 ± 0.83
2453660.8243	13.26 ± 1.03	45.27 ± 0.82
2453661.8003	59.44 ± 1.03	−43.73 ± 0.82
2453662.8240	45.43 ± 1.02	−24.96 ± 0.81
2453663.8200	−8.61 ± 1.17	78.60 ± 0.94
2453664.7964	−9.37 ± 1.04	82.46 ± 0.83
2453678.7838[a]	20.98 ± 1.25	
2453679.7282	63.91 ± 1.09	−50.16 ± 0.88
2453753.6614	−2.29 ± 1.10	70.06 ± 0.88
2453755.6823	55.55 ± 1.14	−37.94 ± 0.91

Note. [a]This phase is close to the conjunction, where only one CCF peak is visible.

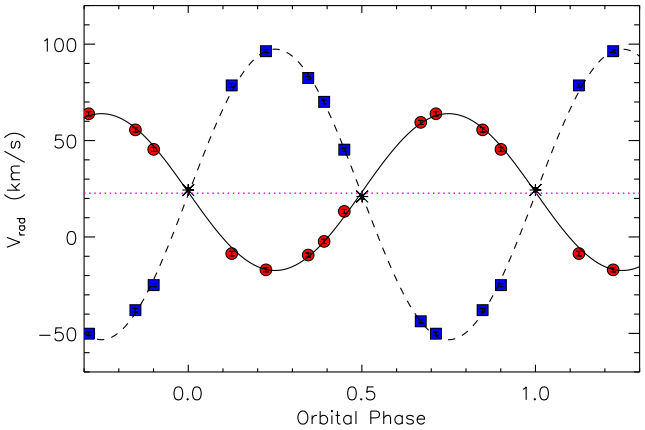

Figure 5. RV curve of the binary system V1481 Ori phased with the orbital period $P = 4.433$ d. Circles and squares refer to the primary and the secondary components, respectively, while asterisks are used when the two components were not resolved in the spectra. The RV errors are also shown and are smaller than the symbol size. The solid and dashed lines represent the circular orbital solutions for the primary and secondary components, respectively, whereas the dotted line is the mean barycentric RV value.

5 ORBITAL AND PHYSICAL PARAMETERS

5.1 Radial velocity

We measured radial velocities (RVs) and their uncertainties following the procedure described in Biazzo et al. (2009), which is based on the analysis of the Cross Correlation Functions (CCFs) between stellar spectra and numerical masks (see that paper for details). In nine spectra, far from the conjunctions, we could resolve both binary components and get their respective RVs from two separate Gaussian fits. In the other two spectra, at phases very close to the conjunctions, we were able to see only one peak in the CCF and to measure blended RVs. Regions containing telluric lines were removed. The RV values of both primary (more massive) and secondary components are listed in Table 5 and plotted in Fig. 5, together with their errors.

We used the RV curves to search for orbital fitting parameters and their uncertainties, following the prescriptions of Lucy &

Table 6. Measured orbital parameters: orbital period (P_{orb}), barycentric velocity (γ), and RV semi-amplitude of the binary components (k^A, k^B).

P_{orb} (d)	4.433
γ (km s^{-1})	22.7 ± 0.3
k^A (km s^{-1})	-40.3 ± 0.5
k^B (km s^{-1})	74.6 ± 0.4

Sweeney (1971) for circular orbits and using the CURVEFIT routine (Bevington 1969) in IDL.[2] Thus, adopting the condition of null eccentricity ($e = 0$), we obtained an orbital period $P_{orb} = 4.433$ d, which is in agreement with the photometric one of 4.4351 d (see Section 4.2) and smaller than the cut-off value of 7.56 d found by Melo et al. (2001) for orbital circularization in pre-main sequence binaries. With this orbital period and the initial heliocentric Julian Day (i.e. HJD0 = 2453658.8320; see Section 4.2) we computed the orbital parameters of the binary system listed in Table 6 (see also Fig. 5).

5.2 Luminosity ratio

Da Rio et al. (2009) measured the following values of magnitudes and colour: $V = 15.153 \pm 0.004$ mag, $I = 12.519 \pm 0.009$ mag, and $V-I = 2.634$ mag. Their I magnitude (obtained with the ESO879 broad-band filter) is not immediately comparable with our Bessel I magnitude. From TiO band they derive an effective temperature $T_{eff} = 3630$ K and a V-band extinction $A_V = 0.334$ mag, and an accretion to total luminosity $Log_{Ac} = -2.95$ for the unresolved system. They compare the HR position of V1481 Ori with different evolutionary models (Da Rio et al. 2010), obtaining for the whole system mass and age in the range from 0.29 $M_\odot$ to 0.72 $M_\odot$ and from 0.4 Myr to 1.4 Myr, using the D'Antona & Mazzitelli (1997) and Baraffe et al. (1998) models, respectively. Da Rio et al. (2012) subsequently obtained the intermediate values $M = 0.42$ $M_\odot$ and age = 1.1 Myr (using Siess, Dufour & Forestini 2000 models) and $M = 0.405$ $M_\odot$ and age = 0.75 Myr (using Palla & Stahler 1999 models). All these results were obtained before the binary nature of the system was known. In contrast to earlier works, we are now in the position to obtain the parameters of the individual components.

The CCF peaks show that the binary components have similar spectral types. When spectral types of binary components are not very different (within one spectral class), the relative intensities of the CCF peaks provide a good proxy of individual stellar fluxes to the combined flux (see Covino et al. 2001, and references therein). Since the stars are components of a binary system, they share the same distance, and therefore the flux ratio provide a good approximation of the luminosity ratio. We can therefore assume that the ratio of the CCF peaks allows us to infer the luminosity ratio L_B/L_A of the components. We find a variable luminosity ratio with an average value of 0.79 between the two components and a mass ratio $M_B/M_A = 0.55$. Evolutionary models can help us to find masses and radii of both components. First, considering the hotspot as the cause of the observed variability, we will use the faintest and reddest magnitude and colour to position the system components on the Magnitude–T_{eff} diagram. Subsequently, we will consider the brightest magnitude and bluest colour to position the components in the diagram.

[2] IDL (Interactive Data Language) is a registered trademark of Exelis Visual Information Solutions.

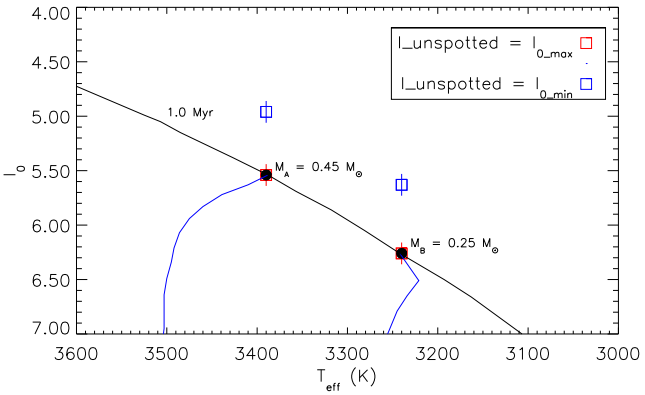

Figure 6. I_0 versus T_{eff} diagram of V1481 Ori. Black and blue solid lines represent theoretical isochrones and mass evolutionary tracks, respectively, from Baraffe et al. (1998). Black bullets represent the magnitudes expected from a model at 1 Myr. Red and blue open squares represent the observed magnitudes in the hypothesis that the unspotted magnitude corresponds to the faintest and brightest observed values, respectively.

We assume that the faintest observed I-band magnitude, $I = 13.05$ mag, represents the unperturbed photosphere, unaffected by either accretion effects or star-spots. Applying the extinction correction, $A_I = 0.16$ mag, which is derived from $A_V = 0.33$ mag, assuming $A_I/A_V = 0.479$ (Cardelli, Clayton & Mathis 1989), and the distance $d = 389.5 \pm 18$ pc (obtained from a weighted mean of the values given by Jeffries 2007, Sandstrom et al. 2007, and Bertout, Robichon & Arenou 1999), we derive the absolute reddening-corrected magnitude $I = 4.94 \pm 0.10$ mag for the unresolved system. We obtain $I = 4.49 \pm 0.10$ mag if we instead assume the brightest observed magnitude corresponds to the star immaculate state.

From our spectroscopic and photometric analysis we know that the orbital and rotation periods are synchronized. Therefore, it is reasonable to assume that both components have same inclination of their rotation axes. In such a case, the ratio between the projected rotational velocities is equal to the ratio between the stellar radii, i.e. $R_B/R_A = 0.84 \pm 0.11$. We can use these observational constraints and the Baraffe et al. (1998) models to find the masses of the individual components. Considering a possible age spread among the ONC members, we used models in the age range from 0.5 to 3 Myr. We find that the measured mass and radius ratios are best reproduced by two stars with masses $M_A = 0.45$ $M_\odot$ and $M_B = 0.25$ $M_\odot$ with radii $R_A = 1.97$ $R_\odot$ and $R_B = 1.57$ $R_\odot$ at an age of 1 Myr and with a luminosity ratio $L_B/L_A = 0.54$.

The model-derived absolute I-band magnitudes and effective temperatures for the two components are $I_A = 5.54$ mag and $I_B = 6.26$ mag and $T_A = 3390$ K and $T_B = 3240$ K (blue squares in Fig. 6). Since the two components are at the same distance from the Sun and have similar spectral types, we assume that the flux ratio $F_B/F_A \simeq L_B/L_A = 0.54$ and, therefore, we can infer the magnitude correction to apply to the observed absolute magnitude ($I = 4.94 \pm 0.10$ mag) to compute the absolute magnitudes of the individual components. Specifically, we obtain $I_A = 5.41 \pm 10$ mag and $I_B = 6.08 \pm 0.10$ mag (red squares in Fig. 6). In contrast to the previous assumption, if we consider the brightest observed magnitude $I = 12.60$ mag as corresponding to the immaculate state, we obtain $I_A = 4.95 \pm 0.10$ mag and $I_B = 5.61 \pm 0.10$ mag, which are irreconcilable with the model values.

The magnitude difference $\Delta I = 0.45 \pm 0.02$ mag between the faintest and brightest state implies that the observed flux, and

consequently the luminosity at the brightest level, is about a factor 1.5 larger than expected from the model. This is in very good agreement with the mean luminosity ratio $L_B/L_A = 0.79$ derived from our spectroscopic analysis, which is a factor 1.5 larger than the value $L_B/L_A = 0.54$ derived from the model. This result is the first clear evidence that the mentioned hotspot is on the secondary component of the system.

Combining stellar radii, projected rotational velocities $v \sin i_A = 19.2 \pm 1.1$ kms^{-1} and $v \sin i_B = 16.1 \pm 0.9$ kms^{-1} measured by Biazzo et al. (2009), and our rotation period we find the inclination of the stellar rotation axes to be $i_A \simeq i_B = 60^\circ$.

Considering that the separation between the components is about 10 solar radii as inferred from the Kepler law (and smaller from surface to surface), which is the typical size of magnetospheres around T Tauri Stars (TTS), and that these magnetospheres are likely interacting, it is unlikely that each component has its own freely orbiting circumstellar disc. Rather the system presumably possesses a circumbinary disc that falls primarily on to the secondary, because its orbit carries it a bit closer to the inner edge of any circumbinary disc with respect to the primary component. Consequently, the secondary component exhibits a hotspot that is responsible for the observed variability of the whole system and makes the component B up to one and a one-half times more luminous than expected from a quiet state.

5.3 Hotspot modelling

To further investigate our hypothesis of a hotspot, we modelled the observed *V*- and *I*-magnitude variations, by selecting the light curve (#14) obtained at the mean epoch HJD 2453668.802 almost simultaneously with the spectroscopic observations. We used the Prsa & Zwitter's (2005) PHOEBE program to simultaneously fit the *V* and *I* light curves, as well as the spectroscopic RV curves. Initial guess values of the spot parameters were obtained after preliminary models of the individual light curves using BINARY MAKER 3.0 (Bradstreet & Steelman 2004). We used as input values the known orbital and physical parameters presented in this Section. The gravity-darkening coefficient has been assumed to be $\nu = 0.25$ (Kopal 1959), and the limb-darkening coefficients from Claret, Diaz-Cordoves & Gimenez (1995) were adopted. Thanks to the dependence of the light curve amplitude on the photometric band wavelength, we could constrain the spot temperature contrast and better determine the area of the spots responsible for the flux rotational modulation. An inspection by eye in the top panel of Fig. 7 immediately reveals that the two light curves do not have the same shape, so it is not a surprise that fitting both equally well failed. On the other hand, the fit to the *V* light curve is satisfactory, in that the models fit all the bumps and wiggles of that curve. However, the same spot in *I*-band flux fails, although it predicts the correct amplitude. We also could successfully fit only the *I*-band flux curve (reduced $\chi^2_V = 0.70$ chi square). However, when we use same parameters for the *V* light curve, they do not fit at all (reduced $\chi^2_I = 2.4$). We have to remind the reader that we are adopting a very simplified scenario, where the observed variability is assumed to be caused by only the hotspots on the secondary component (see bottom panel of Fig. 7). However, since both components are magnetically active, we expect that also cool spots and hot faculae on both components can contribute to the observed variability, revealing the limits of our modelling approach.

The best fit of both curves ($\chi^2_V = 0.70$ and $\chi^2_I = 2.4$) is achieved assuming on the secondary B component a circular spot with radius $r = 20^\circ$ and a temperature contrast $T_{spot}/T_{eff} = 1.13$ ($\Delta T = 420$ K),

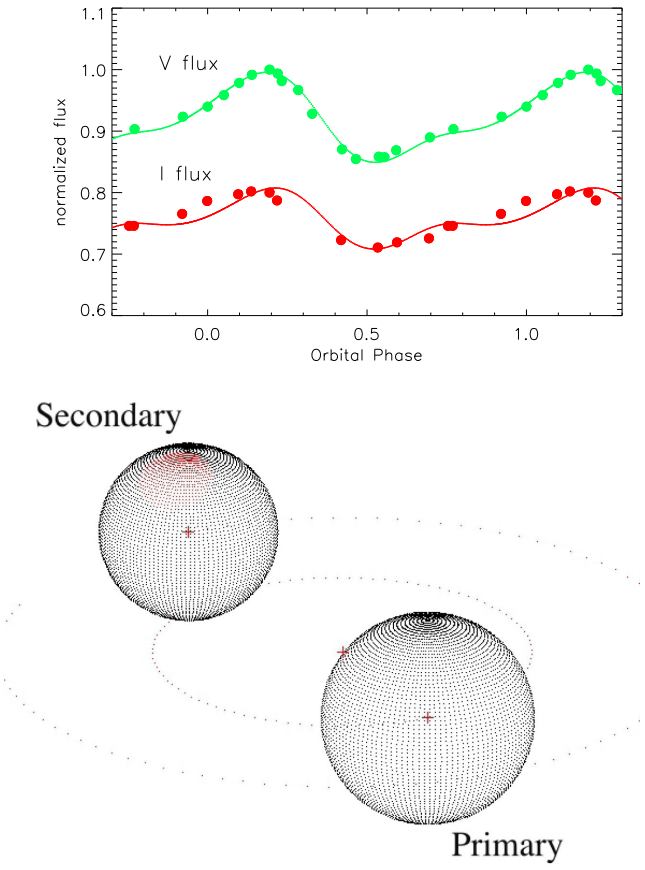

Figure 7. Top: normalized *V* and *I* fluxes (arbitrarily shifted) versus rotation phase at the mean epoch HJD 2453668.802 with overplotted the fit obtained from the hotspot modelling on the secondary component. Bottom: pictorial 3D representation of V1148 Ori with the hotspot on the secondary component. The dotted lines represent the orbital paths of the system components.

whose best visibility is at phase $\phi = 0.13$ (see Fig. 7). Assuming that the excess flux emitted by the hotspot comes from the accretion luminosity, we estimate a lower limit to the mass accretion rate of 9.3×10^{-10} M$_\odot$ yr^{-1}, not implausible for single late-type T Tau stars of similar mass (e.g. Ingleby et al. 2013).

In Fig. 8, we plot, from top to bottom, the RV curves, the L_B/L_A luminosity ratio, and the *V*-band flux curve, which is normalized to the brightest light-curve magnitude, versus the orbital phase. We note a very good correspondence between the luminosity ratio and the *V* light curves. When the flux is maximum, i.e. when the hotspot has best visibility, also the luminosity ratio is maximum. This correspondence supports the presence of the hotspot on the secondary component. The two maxima are at about orbital phase $\phi = 0.19$, which means that the hotspot photo centre is offset by about 70° in longitude from the conjunction of the two components.

Our spot modelling is focused only on the 2005 observation season during which we could also get the spectra. However, an inspection at the top panel of Fig. 3 reveals that brightest, faintest magnitudes, and light-curve amplitude all vary from season to season. Such variations likely correspond to different combinations of area and average latitude of the accretion hotspot. As well, in contrast to the 2005 season, when the variability was dominated by the hotspot, also cool spots may contribute in other seasons to the observed variations.

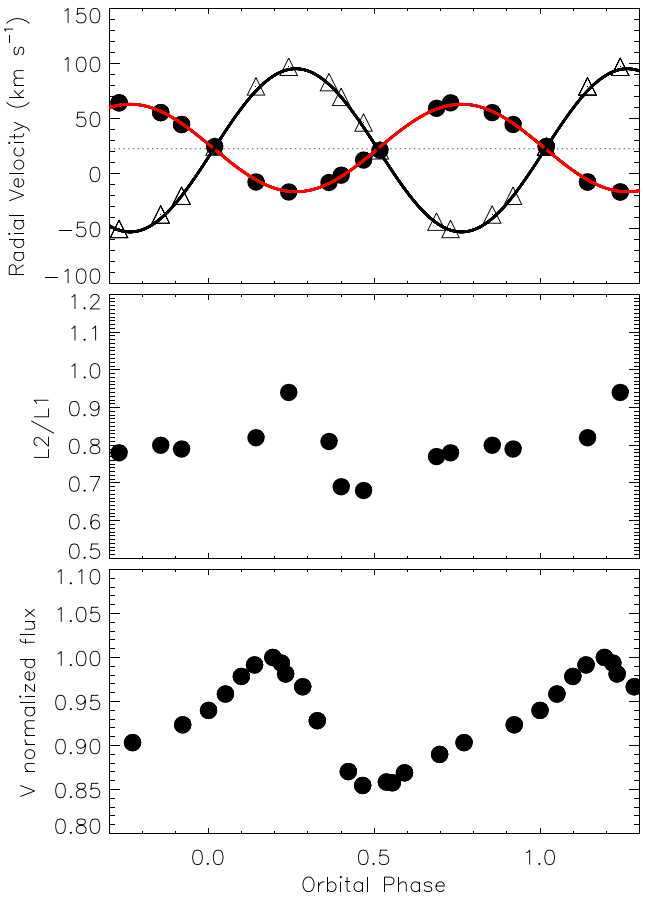

Figure 8. From top to bottom, RV curves, luminosity ratio curve, and *V*-band flux (normalized to the brightest magnitude) versus orbital phase.

6 DISCUSSION

The available data show that the components of V1481 Ori seem to belong to Class II (CTTS). In fact, the H α line, the prominent IR excess, and the presence of an accreting hotspot as inferred from our modelling, are consistent with the existence of a circumbinary accretion disc typical of CTTS stars. Moreover, its optical light-curve amplitude, after correction for the light dilution effect, is $\Delta I > 0.44$ mag ($\Delta V > 0.70$ mag), which is a value observed in CTTS stars, whereas WTTS stars generally exhibit lower amplitudes (see, e.g. Herbst et al. 1994). Despite the stochastic variability generally associated with accretion phenomena, V1481 Ori is one of the known ONC members with the most stable light curves (see Fig. 2). The pooled variance profile shown in Fig. 4 also shows that the variability mostly comes from the rotation and additional variability sources start contributing at much longer time-scales (>3 yr). This behaviour suggests that the secondary component of V1481 Ori has an accretion disc though the accretion is moderate and quite stable; or, that the accretion from a circumbinary disc is primarily on to the secondary, as models suggest.

Our measurements of the luminosity ratio show that it is variable in the range from 0.68 to 0.94. This variation is correlated to the orbital phase and can be accounted by a hotspot covering about 3.5 per cent of the photosphere. However, the minimum value 0.69 is about 30 per cent larger than expected in the case of no accretion. This means that we must invoke the presence of an additional component of bright regions that are quite visible at all phases and therefore not undergoing rotational modulation. In this case, the shape of the hotspot must be quite more complicated than that we could model. We can image that the infalling gas from the disc produces a quite uniform bright belt at the latitude where the hotspot is located, with superimposed the hotspot.

The existence of a circumbinary disc that is accreting material on the secondary component gives a strong observational support to the models of Artymowicz & Lubow (1996). These models predict that, in the case of close T Tauri binaries with low eccentricity and with unequal component masses, the mass flow from the circumbinary disc occurs preferentially on to the lower mass object. Our findings, on the contrary, give less support to other models, e.g. by de Val-Borro et al. (2011), that predict the accretion to occur on both components, although we cannot rule out the presence of at least some accretion on to the primary.

Fully convective stars such as V1481 Ori are expected to rotate as a solid body. Indeed, we do not detect any evidence of SDR from seasonal rotation period variations at the 0.7 per cent level, which is the 3σ precision of our rotation period measurements. On the other hand, young main-sequence stars with a rotation period of about 5 d generally exhibit variations of the measured photometric rotation period $\Delta P/P$ up to 5 per cent, which are attributed to SDR (e.g. Messina & Guinan 2003). What we unexpectedly found is a possible slow oscillation of the phase of maximum with period of about 6 yr. Such an oscillation can arise from a variation of the angular velocity with which the hotspot producing the light modulation is carried out across the photosphere. This angular velocity exhibits a variation $\Delta\Omega/\Omega = 0.065$ per cent, which is a factor 20 smaller than the precision with which our measurements can reveal rotation period variations. This may be a nice example case of how powerful the analysis of phase migration of light-curve minima in SDR studies can be. The angular velocity variation we observed can be due to a periodic latitude migration of the hotspot on a differentially rotating star. In this case, we measure a lower limit to the amplitude of SDR, since the latitude interval spanned by the hotspot is limited.

Because our star is probably locked to its accretion disc by its strong magnetic field, an alternative explanation is that the disc and the star exchange angular momentum back and forth in a cyclic fashion. In this case, assuming the stellar parameters given above and an internal structure as a polytrope of index $n = 3/2$, we can estimate the minimum magnetic field strength required to transfer a sufficient amount of angular momentum during an oscillation period to account for the observed amplitude (see Appendix A). We find a minimum field strength of about 650 G at the stellar surface, that is in agreement with the strong surface fields found in T Tau stars.

7 CONCLUSIONS

We have carried out a photometric and spectroscopic study of the SB2 spectroscopic binary V1481 Ori, a member of the ONC. Spectroscopic data were collected at the ESO/VLT and photometric data were collected at the IAO since 2004. The latter were complemented with photometric observations performed at VVO since 1991, totalling a series of about 20 yr of *I*-band photometry. Our spectroscopic analysis has allowed us to confirm the binary nature of this system, obtaining the RV curves of both components, from which we derived the orbital period $P_{\rm orb} = 4.433$ d, the mass ratio $M_{\rm B}/M_{\rm A} = 0.54$, and the luminosity ratio $L_{\rm B}/L_{\rm A}$, which is found to vary with orbital phase. A comparison with evolutionary models from Baraffe et al. (1998) allowed us to infer masses $M_{\rm A} = 0.45$ M$_\odot$ and $M_{\rm B} = 0.25$ M$_\odot$ and radii $R_{\rm A} = 1.97$ R$_\odot$ and

$R_B = 1.57\ R_\odot$ of both components, and the inclination of the rotation axes $i_A \simeq i_B = 60^\circ$.

The analysis of photometric data has allowed us to detect a very stable light modulation with an average period $P_{rot} = 4.4351$ d that we attribute to the presence of a hotspot, which is presumably generated by material accreting from a circumbinary disc on to the lower mass component, and is carried in and out of view during the orbital revolution. Although both components are expected to host some level of magnetic activity (starspots) due to the deep convection zone and the fast rotation, the observed variability arising from this hotspot seems to be dominant with respect to any additional contribution from cool spots. The presence of a hotspot on the secondary component is also found by our modelling of the multiband light curves and RV curves collected in the 2005 season.

We find that luminosity ratio variations correlate very well with the *I*-band flux variations, in the sense that the maximum luminosity ratio is observed at the same phases (0.2–0.3) that the light curve has its maximum. This circumstance gives strong support to the presence of a hotspot as cause of the observed variability. The hotspot is located at about 70 deg from the substellar longitude. Our findings favour those accretion models predicting, in the case of close T Tauri binaries with low eccentricity and with unequal component masses, the mass flow from the circumbinary disc to occur preferentially on to the lower mass object.

From the migration in phase of the light-curve maximum, we infer a variation of the photometric period of 0.065 per cent. That is very close to rigid-body rotation, as expected by the models mentioned in the Introduction. We find an interesting periodic oscillation of about 6 yr that can arise from a variation of the angular velocity with which the hotspot producing the light modulation is carried out across the photosphere. The angular velocity variation we observed can be due to a periodic latitude migration of the hotspot on a differentially rotating star. An alternative explanation is that the disc and the star exchange angular momentum back and forth in a cyclic fashion. In this case, we find a minimum required field strength of about 650 G at the stellar surface, that is in agreement with the strong surface fields found in T Tau stars.

ACKNOWLEDGEMENTS

The work is based on data collected at the Indian Institute of Astrophysics (IIA) and European Southern Observatory (ESO). The extensive use of the SIMBAD and ADS databases operated by the CDS centre, Strasbourg, France, is gratefully acknowledged. The authors thank the anonymous Referee for helpful comments that allowed to improve the quality of the manuscript.

REFERENCES

Artymowicz P., Lubow H. S., 1996, ApJ, 467, 77
Attridge J., Herbst W., 1992, ApJ, 398, L61
Baraffe I., Chabrier G., Allard F., Hauschildt P. H., 1998, A&A, 337, 403
Barnes J. R., Collier Cameron A., Donati J.-F., James D. J., Marsden S. C., Petit P., 2005, MNRAS, 357, L1
Bertout C., Robichon N., Arenou F., 1999, A&A, 352, 574
Bevington P. R., 1969, Data Reduction and Error Analysis for the Physical Sciences. McGraw-Hill, New York
Biazzo K., Melo C. H. F., Pasquini L., Randich S., Bouvier J., Delfosse X., 2009, A&A, 508, 1301
Blecha A., Cayatte V., North P., Royer F., Simond G., 2000, in Iye M., Moorwood A. F., eds, Proc. SPIE Conf. Ser. Vol. 4008, Optical and IR Telescope Instrumentation and Detectors. SPIE, Bellingham, p. 367
Bradstreet D. H., Steelman D. P., 2004, Binary Maker 3: Light Curve Synthesis Program. Norristown. Contact Software, 19041
Cardelli J. A., Clayton G. C., Mathis J. S., 1989, ApJ, 345, 245
Claret A., Diaz-Cordoves J., Gimenez A., 1995, A&AS, 114, 247
Cohen R. E., Herbst W., Williams E. C., 2004, AJ, 127, 1602
Collier Cameron A., 2007, Astron. Nachr., 328, 1030
Covino E., Melo C., Alcalá J. M., Torres G., Fernández M., Frasca A., Paladino R., 2001, A&A, 375, 130
Cutri R. M., Wright E. L., Conrow T. et al., 2013, The IRSA 2MASS All-Sky Point Source Catalog, NASA/IPAC Infrared Science Archive
D'Antona F., Mazzitelli I., 1997, Mem. Soc. Astron. Ital., 68, 807
Da Rio N., Robberto M., Soderblom D. R., Panagia N., Hillenbrand L. A., Palla F., Stassun K., 2009, ApJS, 183, 261
Da Rio N., Robberto M., Soderblom D. R., Panagia N., Hillenbrand L. A., Palla F., Stassun K. G., 2010, ApJ, 722, 1092
Da Rio N., Robberto M., Hillenbrand L. A., Henning T., Stassun K. G., 2012, ApJ, 748, 14
de Val-Borro M., Gahm G. F., Stempels H. C., Peplin'ski A., 2011, MNRAS, 413, 2679
Dobson A. K., Donahue R. A., Radick R. R., Kadlec K. L., 1990, in Wallerstein G., ed., ASP Conf. Ser. Vol. 9, The Sixth Cambridge Symposium on Cool Stars, Stellar Systems and the Sun. Astron. Soc. Pac., San Francisco, p. 132
Donahue R. A., Baliunas S. L., 1992, ApJ, 393, L63
Donahue R. A., Dobson A. K., Baliunas S. L., 1997, Sol. Phys., 171, 191
Edwards S. et al., 1993, AJ, 106, 372
Feigelson E. D., Broos P., Gaffney J. A., Garmire G., Hillenbrand L. A., Pravdo S. H., Townsley L., Tsuboi Y., 2002, ApJ, 574, 258
Furesz G., Hartmann L. W., Megeath S. T., Szentgyorgyi A. H., Hamden E. T., 2008, ApJ, 676, 1109
Gagne M., Caillault J.-P., Stauffer J. R., 1995, ApJ, 445, 280
Geier S., Wendker H. J., Wisotzki L., 1995, A&A, 299, 39
Getman K. V. et al., 2005, ApJS, 160, 319
Grankin K. N., Melnikov S. Yu., Bouvier J., Herbst W., Shevchenko V. S., 2007, A&A, 461, 183
Grankin K. N., Bouvier J., Herbst W., Melnikov S. Yu., 2008, A&A, 479, 827
Herbst W., Herbst D. K., Grossman E. J., Weinstein D., 1994, AJ, 108, 1906
Herbst W., Rhode K. L., Hillenbrand L. A., Curran G., 2000, AJ, 119, 261
Hillenbrand L. A., 1997, AJ, 113, 1733
Hillenbrand L. A., Strom S. E., Calvet N., Merrill K. M., Gatley I., Makidon R. B., Meyer M. R., Skrutskie M. F., 1998, AJ, 116, 1816
Ingleby L. et al., 2013, ApJ, 767, 112
Jeffries R. D., 2007, MNRAS, 376, 1109
Johns-Krull C. M., 1996 A&A, 306, 803
Jones B. F., Walker M. F., 1988, AJ, 95, 1755
Kazarovets E. V., Samus N. N., Durlevich O. V., 2001, Inf. Bull. Var. Stars, 5135
Kopal Z., 1959, Close Binary Systems. Chapman and Hall, London
Küker M., Rüdiger G., 1997, A&A, 328, 253
Küker M., Stix M., 2001, A&A, 366, 675
Lamm M. H., Bailer-Jones C. A. L., Mundt R., Herbst W., Scholz A., 2004, A&A, 417, 557
Lanza A. F., 2007, A&A, 471, 1011
Lucy L. B., Sweeney M. A., 1971, AJ, 76, 544
Melo C. H. F., Covino E., Alcalá J. M., Torres G., 2001, A&A, 378, 898
Messina S., Guinan E. F., 2003, A&A, 409, 1017
Palla F., Stahler S. W., 1999, ApJ, 525, 772
Parenago P. P., 1954, Publ. Astron. Inst. Sternberg, 25, 393
Parihar P., Messina S., Distefano E., Shantikumar N. S., Medhi B. J., 2009, MNRAS, 400, 603
Prsa A., Zwitter T., 2005, ApJ, 628, 426
Rebull L. M., Stauffer J. R., Megeath S. T., Hora J. L., Hartmann L., 2006, ApJ, 646, 297
Rice J. B., Strassmeier K. G., 1996, A&A, 316, 164
Rodriguez-Ledesma M. V., Mundt R., Eisloeffel J., 2010, A&A, 515, A13

Rosino L., 1956, Mem. Soc. Astron. Ital., 27, 335
Sandstrom K. M., Peek J. E. G., Bower G. C., Bolatto A. D., Plambeck R. L., 2007, ApJ, 667, 1161
Scargle J. D., 1982, ApJ, 263, 835
Sicilia-Aguilar A. et al., 2005, AJ, 129, 363
Siess L., Dufour E., Forestini M., 2000, A&A, 358, 593
Stassun K. G., Mathieu R. D., Mazeh T., Vrba F. J., 1999, AJ, 117, 2941
Tobin J. J., Hartmann L., Furesz G., Mateo M., Megeath S. T., 2009, ApJ, 697, 1103
Werner M. W. et al., 2004, ApJS, 154, 1

SUPPORTING INFORMATION

Additional Supporting Information may be found in the online version of this article:

Table 2. (http://www.mnras.oxfordjournals.org/lookup/suppl/doi:10.1093/mnras/stv3000/-/DC1).

Please note: Oxford University Press is not responsible for the content or functionality of any supporting materials supplied by the authors. Any queries (other than missing material) should be directed to the corresponding author for the article.

APPENDIX A: MAGNETIC COUPLING BETWEEN A STAR AND ITS DISC: ANGULAR MOMENTUM EXCHANGE

The variation of the spin angular momentum of the star L is given by

$$\frac{\mathrm{d}L}{\mathrm{d}t} = \tau, \tag{A1}$$

where t is the time and τ the torque due to the Maxwell stresses produced by the magnetic field that couples the star with its disc. The torque applied at the surface of the star is given by the integral of the Maxwell stress $B_r B_\phi$ applied there (cf. Lanza 2007):

$$\tau = -\frac{1}{\mu}\int_S R \sin\theta B_r B_\phi \,\mathrm{d}S, \tag{A2}$$

where μ is the magnetic permeability of the plasma, R is the radius of the star, θ is the colatitude measured from the North pole, B_r is the radial and B_ϕ is the azimuthal component of the magnetic field at the surface of the star, and S is the stellar surface. Assuming that the field components are axisymmetric, we obtain

$$\tau = -\frac{\pi^2}{\mu} R^3 \langle B_r B_\phi \rangle, \tag{A3}$$

where the brackets indicate the mean value of the Maxwell stress over the surface of the star. If the magnetic stresses modulate the angular velocity Ω of the star with a period $P_{\rm mod}$, the amplitude of the variation of the angular momentum is given by

$$\frac{\mathrm{d}L}{\mathrm{d}t} = \frac{2\pi I}{P_{\rm mod}} \Delta\Omega, \tag{A4}$$

where I is the moment of inertia of the star and $\Delta\Omega$ is the amplitude of its angular velocity modulation assumed to oscillate sinusoidally as a function of the time. The moment of inertia of the star can be written as $I = kMR^2$, where $k = 0.205$ for a polytrope of index $n = 3/2$, is a constant depending on the density stratification inside the star and M is the mass of the star. Considering equations (A1), we can equate the right-hand sides of (A3) and (A4) and with some re-arrangement of the terms we obtain

$$\langle B_r B_\phi \rangle = \frac{2k\mu}{\pi R P_{\rm mod}} M \Delta\Omega, \tag{A5}$$

that we use to estimate the Maxwell stress at the surface of the star. The minimum magnetic field strength $B_{\rm min}$ corresponds to the case when $B_r = B_\phi$ and is given by $B_{\rm min} = (\langle B_r B_\phi \rangle)^{1/2}$.

This paper has been typeset from a TEX/LATEX file prepared by the author.